# Laboratori Nazionali di Frascati

Submitted to Nucl. Instr. & Meth. in Phys. Res.

LNF-93/034 (P)
5 Luglio 1993

A.Antonelli, R.Baldini, A.Balla, C.Becciani, M.Bertani, M.E.Biagini, C.Bini, V.Bidoli, T.Bressani, R.Calabrese, R.Cardarelli, R.Carlin, C.Casari, R.Chiaratti, L.Cugusi, P.Dalpiaz, S.De Simone, G.De Zorzi, A.Di Virgilio, A.Feliciello, M.L.Ferrer, P.Ferretti Dalpiaz, P.Gauzzi, P.Gianotti, R.Giantin, S.Guiducci, F.Iazzi, E.Luppi, S.Marcello, A.Masoni, R.Messi, B.Minetti, M.Morandin, L.Paoluzi, E.Pasqualucci, G.Pauli, F.Petrucci, A.Pia, G.Pitacco, M.Posocco, M.A.Preger, G.Puddu, L.Santi, R.Santonico, P.Sartori, M.Savrie', S.Serci, M.Spinetti, L.Tecchio, S.Tessaro, C.Voci:

## THE FENICE DETECTOR AT THE $e^+e^-$ COLLIDER ADONE

PACS.: 29.40.Vj

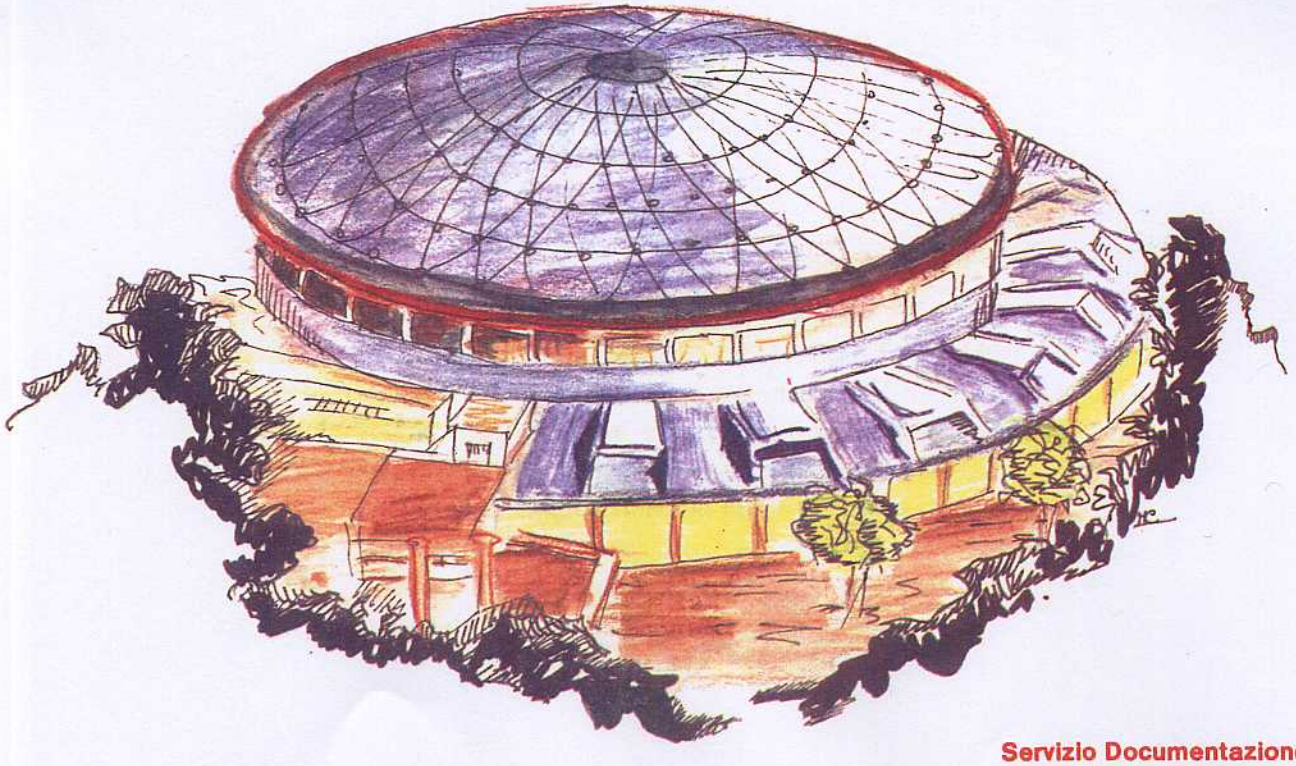

Servizio Documentazione
dei Laboratori Nazionali di Frascati
P.O. Box, 13 - 00044 Frascati (Italy)

INFN - Laboratori Nazionali di Frascati
Servizio Documentazione

LNF-93/034 (P)
5 Luglio 1993

# THE FENICE DETECTOR AT THE $e^+e^-$ COLLIDER ADONE

A.Antonelli[a], R.Baldini[a], A.Balla[a], C.Becciani[b], M.Bertani[c], M.E.Biagini[a], C.Bini[d], V.Bidoli[e], T.Bressani[f], R.Calabrese[c], R.Cardarelli[e], R.Carling, C.Casari[h], R.Chiarattig, L.Cugusi[h], P.Dalpiaz[c], S.De Simone[a], G.De Zorzi[d], A.Di Virgilio[a], A.Feliciello[f], M.L.Ferrer[a], P.Ferretti Dalpiaz[c], P.Gauzzi[d], P.Gianotti[f], R.Giantin[g], S.Guiducci[a], F.Iazzi[f], E.Luppi[c], S.Marcello[f], A.Masoni[h], R.Messi[e], B.Minetti[f], M.Morandin[g], L.Paoluzi[e], E.Pasqualucci[e], G.Pauli[b], F.Petrucci[c], A.Pia[f], G.Pitacco[g], M.Posocco[g], M.A.Preger[a], G.Puddu[h], L.Santi[i], R.Santonico[e], P.Sartori[g], M.Savrie'[c], S.Serci[h], M.Spinetti[a], L.Tecchio[f], S.Tessaro[b], C.Voci[g]

[a]INFN Laboratori Nazionali di Frascati, Frascati, Italy,
[b]Università di Trieste and INFN Sezione di Trieste, Trieste, Italy
[c]Università di Ferrara and INFN Sezione di Ferrara, Ferrara, Italy
[d]Università La Sapienza and INFN Sezione di Roma I, Roma, Italy
[e]Università di Tor Vergata and INFN Sezione di Roma II, Roma, Italy
[f]Università, Politecnico and INFN Sezione di Torino, Torino, Italy
[g]Università di Padova and INFN Sezione di Padova, Padova, Italy
[h]Università di Cagliari and INFN Sezione di Cagliari, Cagliari, Italy
[i]Università di Udine and INFN Gruppo Collegato di Udine, Udine, Italy

## ABSTRACT

The FENICE detector, installed at the Frascati $e^+e$ storage ring ADONE, for measuring the neutron e.m. form factors in the time–like region, is described. FENICE is a non magnetic detector and consists of a complex array of scintillators, limited streamer tubes and iron converters for detecting mainly the process $e^+e^- \rightarrow \bar{n}n$. Antineutrons are identified by the charged prongs produced in their annihilation and the antineutron velocity is measured by the retrieved annihilation time respect to the beam crossing time. Neutrons are detected in plastic scintillator layers. To reduce the cosmic rays background a concrete shield, covered by an active veto system, is added.

## 1. – INTRODUCTION

A consistent set of measurement of nucleon e.m. form factors (FF) is not available up to now. While the proton space–like and time–like FF are measured, there are few data on the neutron space–like FF [1, 2, 3, 4] and the neutron time–like FF have never been measured. Only an upper limit at $\sqrt{s} = 2.4$ GeV issued by DM2 collaboration [5] has been obtained up to now.

The main goal of the FENICE experiment is to measure the neutron FF in the time–like region, that is to measure the cross section for $e^+e^- \rightarrow \bar{n}n$ in the c.m. energy range from threshold up to 3.1 GeV [6]. This measurement is a crucial test for the current nucleon models which all reproduce the proton and neutron space–like FF, but are in disagreement in providing the cross section for $e^+e^- \rightarrow \bar{n}n$ [7]. A suitable quantity to compare the theoretical predictions is the ratio between the total cross sections:

$$R = \sigma(e^+e^- \rightarrow \bar{n}n)/\sigma(e^+e^- \rightarrow \bar{p}p)$$

The expected value from PQCD is $R \cong 0.25$, whereas EVMD (Extended Vector Meson Dominance Model) predictions range from 1 to 100 depending on the number of poles, and some Skyrme–like models predict a ratio decreasing according to $1/Q^4$ [8, 9].

The experiment has started its data taking in 1991 at ADONE [10] in Frascati. ADONE is a conventional $e^+e^-$ collider that works in the energy range $1.5\ \text{GeV} < E_{cm} < 3.1\ \text{GeV}$. The average luminosity is $\sim 10^{29}\ \text{cm}^{-2}\ \text{s}^{-1}$ with a total current of 10–25 mA; in these conditions the mean life of the beam is ~ 4 hours.

The overall apparatus (Fig. 1a) is 2.5 m long, 3 m large and has an octagonal cross

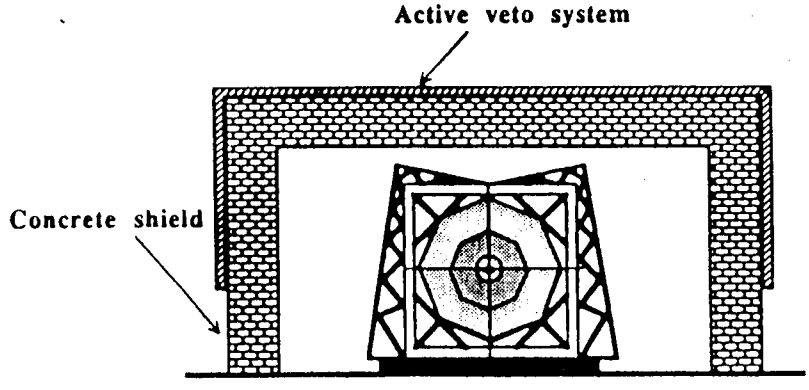


**FIG. 1a** – Schematic view of the FENICE detector: the concrete shield is also shown.

section. It is a non magnetic detector and it covers $0.76 \times 4\pi$ sr ($\phi$ acceptance of $1.8\pi$ rad and $|\cos\vartheta| < 0.848$) for a particle traversing the whole detector and coming from the $e^+e^-$ interaction region. The total thickness corresponds to about 8 radiation lengths and to a number of collision lengths that ranges from 1.2 to 5 depending on the energy.

Mechanically the apparatus consists of four super modules which have individual support frames and can be moved on rails in order to open the detector.

Starting from the beam pipe there are four dedicated parts with separate functions: the Central Tracking Detector (CTD), the neutron detector, the antineutron detector and the cosmic ray shield.

## 2. – THE ANTINEUTRON DETECTOR

The identification of the $\bar{n}$ is performed by means of annihilation in matter exploiting the many prongs topology of the event and the time of flight (TOF) corresponding to the reconstructed vertex with respect to the beam crossing time. Therefore for each $n\bar{n}$ candidate, the $\bar{n}$ velocity ($\beta$) is determined. For the $\bar{n}$ detector we have chosen a structure similar to that developed by the PS178 experiment at LEAR [11, 12] which studied the reaction $\bar{p}p \rightarrow \bar{n}n$.

The basic module is composed interleaving 4 iron plates, 5 mm thick, as main converter, with 4 limited streamer tubes (LST) layers as tracking detector [13, 14]. A 20 mm thick scintillation counter hodoscope is added for triggering and TOF measurements. The full module is repeated four times and after the last hodoscope two more LST planes are added. A schematic view of a supermodule, in a plane perpendicular to the beam axis, is shown in Fig. 1b.

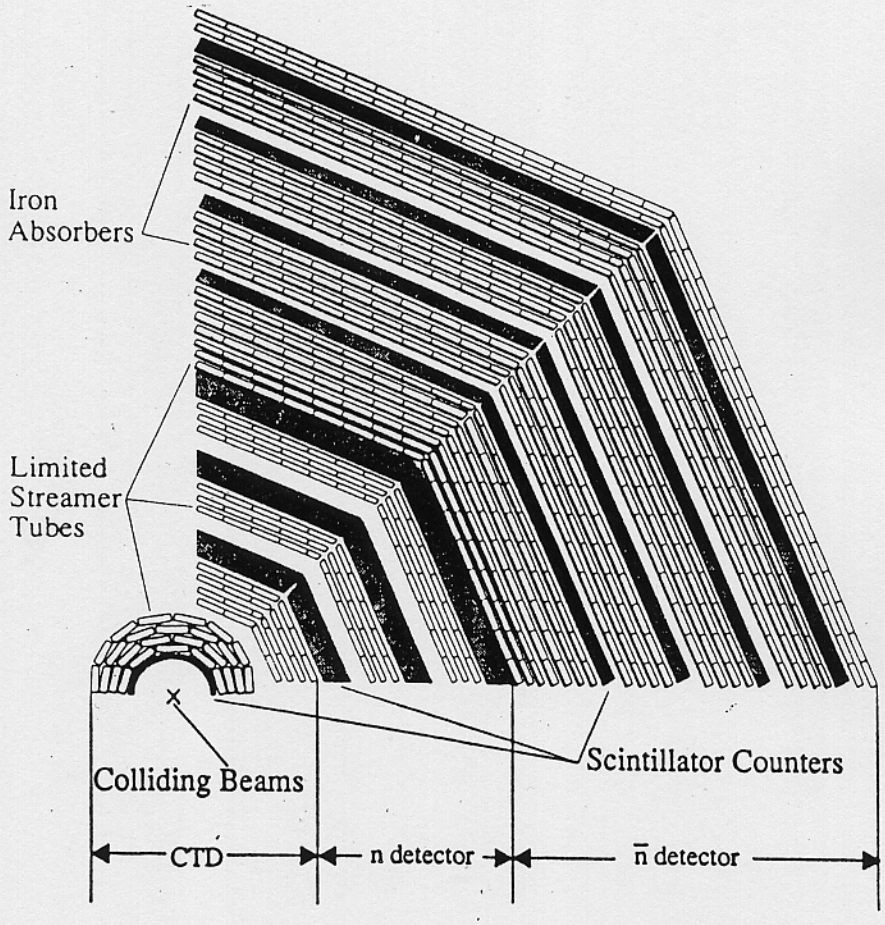


**FIG. 1b** – Detailed view of the FENICE detector showing two contiguous octants.

The LST chamber consists of a plastic (PVC) comb profile having 8 or 7 cells arranged in a layer to leave as little dead space as possible. Each cell has an inner dimension of 0.9x0.9 cm$^2$. The internal surface of the comb is painted with graphite. Each profile is inserted in a plastic box to insure the gas tightness. Wires 100 μm in diameter run along the cell axis and are parallel to the beam axis. They are soldered at both extremities on printed circuits cardboards. One of them supplies the positive high voltage to wires. The LSTs are flushed with a gas

mixture of 30% argon and 70% isobutane. At 4.6 KV the pulses on the wire are ~ 50 mV/50 Ω in amplitude, with a ~ 5 ns rise time and ~ 30 ns FWHM. We do not collect directly the signal from the wire: on both sides of the comb profile the streamers induce pulses on external aluminum strips placed along the wires (X strips) and across the wires (Y strips). This system provide a bidimensional measurement of the point along the track. The X strips have 10 mm pitch and are 4 mm wide, the Y strips have 12 mm pitch and are 1 cm wide. Spatial resolutions of 2.3 mm and 3.5 mm respectively were measured. The strips are digitally read out by dedicated integrated electronics, manufactured by SGS, which converts the pulses into a 1μs long digital signal that is latched into one bit of a shift register. The shift registers are daisy chained together in groups of 640 elements and the readout is performed by a Camac controller (STROC) [15].

The sensitive length of the scintillator counters is 2.4 m, with the exception of the two lower octants, which have shorter tubes and scintillators (1.9 m) due to the supports of machine's quadrupoles. The width of a counter ranges from 33 to 26 cm to minimize the dead space. Each counter, made of NE110 scintillator, is viewed on both ends by THORN–EMI 9813KB photomultipliers glued on a light guide. The mechanical housing of the PM bases was made by light black plastics and only a light μ–metal shield was used in order to have the minimum weight to be supported by the glue. This technique was adopted following careful inspection of the straight magnetic field along the quadrupoles and a 2 months endurance test of some prototypes. After some initial failures, due to bad gluing of some elements, the full system of PMs had no more failures.

The signal from each PM is splitted through a fan–out module and supplies a TDC, an ADC and is processed by the trigger electronics. The TDC and ADC stability is monitored run by run using cosmic rays while the high voltage stability is ensured within 0.5% by the CAEN SY127 power supplies system. The ADC pedestals are periodically checked and automatically subtracted during readout operations. The TOF absolute calibration of the various counters is performed using $e^+e^-$ and $\mu^+\mu^-$ events. The resolution that we obtain after applying the proper correction for the "time walk", has a σ of 0.7 ns which includes the ~ 0.4 ns spread in crossing time due to the bunch length. On the other hand the overall resolution on the antineutron velocity is dominated by the uncertainty on the path length and on the position of the reconstructed vertex. In Fig. 2a and 2b the 1/β distributions for $e^+e^- \rightarrow n\bar{n}$ and $p\bar{p}$ respectively [16] at the c.m. energy of 3.1 GeV are shown. The obtained distributions, fitted with a gaussian, have a σ of 0.3.The distribution of the $\bar{n}$ annihilation vertex ($R_v$) in the transverse plane for $e^+e^- \rightarrow n\bar{n}$ is in good agreement with Montecarlo expectations, as shown in Fig. 3.

The measured energy resolution of the calorimeter for electromagnetic showers is obtained from $e^+e^- \rightarrow e^+e^-$ events at different energies. For showers with an axis in the range from –0.3 $< \cos\theta < 0.3$ with respect to the beam, we have $\frac{\sigma_E}{E} = 21\%$ at 1GeV with a linearity shown in Fig. 4. The energy resolution for hadronic showers is $\frac{\sigma_E}{E} = \frac{50\%}{\sqrt{E}}$ as measured by the total number of fired strips for multi–hadronic events. These figures allow a good rejection of the machine background events from the $\bar{N}N$ annihilation events.

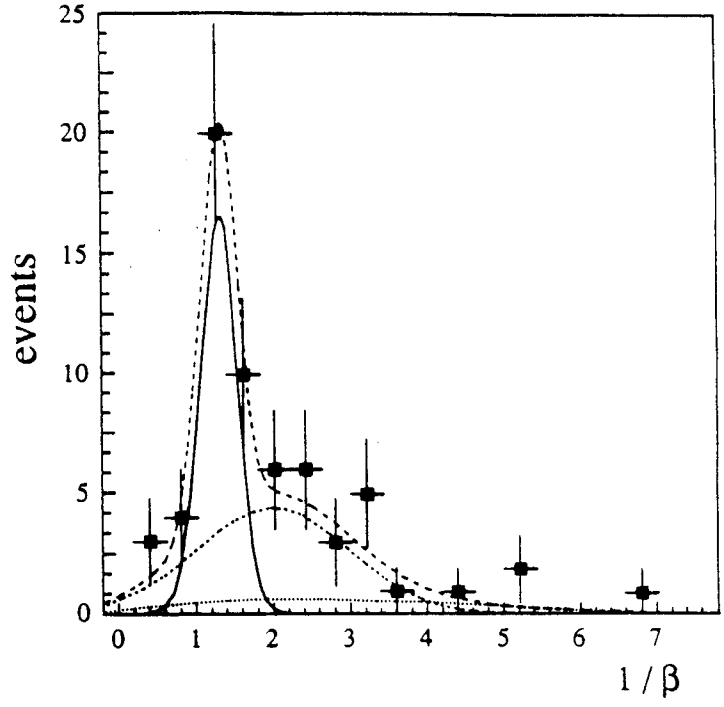


**FIG. 2a** – $1/\beta$ distribution for $e^+e^- \rightarrow \bar{n}\,n$ selected events at 3100 MeV.[16]. The distribution is fitted with a gaussian plus a polynomial background. The continuos curve is the prediction for genuine $e^+e^- \rightarrow \bar{n}\,n$ candidates. The dot–dashed line represent the background contribution $e^+e^- \rightarrow \bar{n}\,n\,(\pi^0,\eta)$, the dotted one is the background due to cosmic rays and the dashed line is the oveall fit to the data.

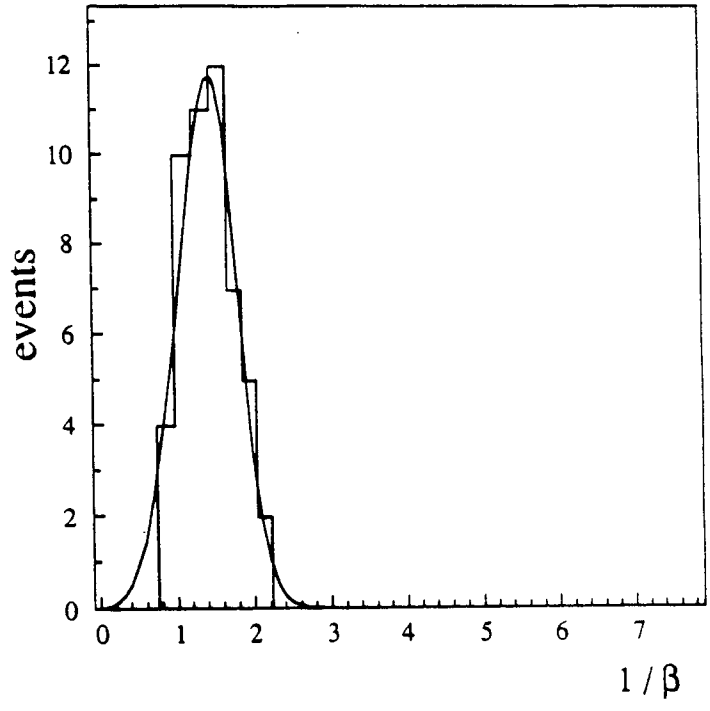


**FIG. 2b** – $1/\beta$ distribution for $e^+e^- \rightarrow \bar{p}\,p$ selected events at 3100 MeV.[16]. The distribution is fitted with a gaussian, since the background for this channel turns out to be negligible.

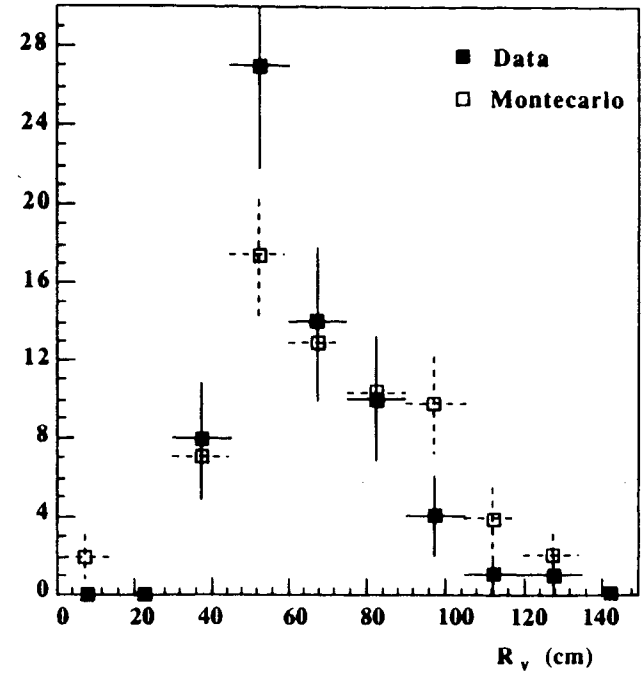


**FIG. 3** – Distribution of the distance from the interaction point Rv in the transverse plane of the reconstructed $\bar{n}$ vertex for candidate events (full squares) and for Montecarlo events (open squares).

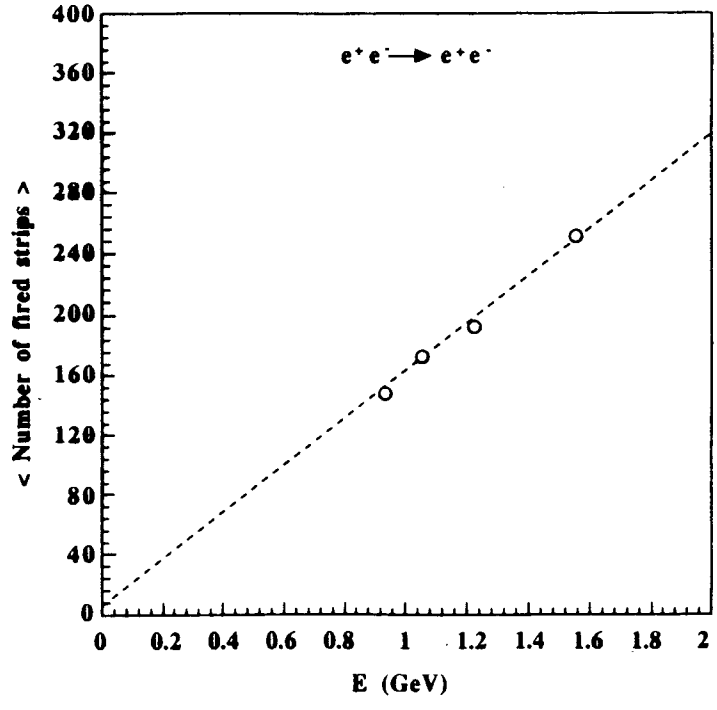


**FIG. 4** – Average number of fired strips as a function of the beam energy for electrons. The response turns out to be linear in the explored range.

## 3. – THE NEUTRON DETECTOR

The neutron detection is a difficult task if one wants to preserve efficiency, timing and position requirements at the same level as for antineutrons. We have adopted a solution of relatively thick scintillaton counter hodoscope, where the NE110 scintillator acts as a converter as well as active material. We have a three layers hodoscope with a total thickness of 15 cm, following the same octagonal structure of the antineutron detector (Fig. 1b). Since the $\bar{n}$ annihilates also in the neutron detector three layers of LST have been added between the scintillators to detect the annihilation products.

The neutron detection efficiency in NE110 scintillator has been measured at the Legnaro National Laboratory using a 2–16 MeV neutron beam [17] from d + d and d + T reactions, and checked by FENICE experiment at high energies. This last measurement was performed using the $J/\Psi \rightarrow \bar{n}n$ and $e^+e^- \rightarrow n\bar{n}$ at $E_{c.m.}$=2.0 GeV, selected by looking at the antineutron only [16]. In Fig. 5 the neutron detection efficiency is shown as a function of neutron kinetic energy for ~ 15 cm thick scintillator. The decrease in efficiency at low energy is also due to the threshold put on the PM signals to avoid background, corresponding to a ~ 4 MeV proton equivalent energy. In our energy range the efficiency flattens out to 1% per centimeter of scintillator [18]. Due to this low efficiency no request is asked for the neutron detection at trigger and selection levels. Nevertheless in a small sample of events the neutron is detected, allowing an important check in the analysis of the $\bar{n}n$ collected events.

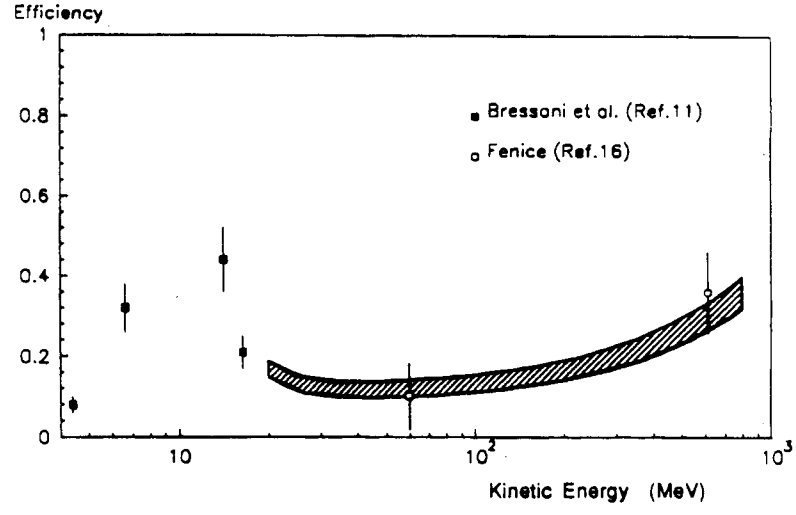


**FIG. 5** – Neutron detection efficiency as a function of the neutron kinetic energy. The shaded area corresponds to the GEANT 3.14 code [23] prediction.

## 4. – THE CENTRAL TRACKING DETECTOR

The aim of the Central Tracking Detector (CTD) is to measure with accuracy charged tracks and their production vertex. Moreover it helps in the selection of $\bar{n}$ n events from $\mu^+\mu^-$, Bhabha scattering, multi–hadrons and in better recognizing $\bar{n}$ annihilations with prongs back to the center of the apparatus. For simplicity the tracking elements are the same LST as before equipped with X and Y strips. The CTD is divided in two substructure: the first close to the pipe and the second just in front to the neutron counter. Each substructure has four LST planes in order to record at least two hits per track and solve partially ambiguities when two tracks

cross the same cell in a layer. The inner substructure consits of a 7 cells chamber to fit the pipe diameter. The standard spatial resolution given by the strips is not sufficient in this case to reconstruct a vertex with an accuracy comparable to the beam transversal dimension (~1x0.1 $mm^2$). To improve the resolution, while keeping the simplicity and reliability of LST, for each tube the drift time across the cell is measured achieving ~ 1 mm resolution compatible with the beam transverse dimensions. The signals from LST of CTD participate to the second level trigger logic.

A layer of 10 scintillators (5 mm thick) is inserted between the pipe and the first tracking substructure. The active length is 1 m and they are equipped with 2 XP2020 photomultipliers at both ends. The signals of these counters participate to the trigger logic and their time of flight measurements are useful to improve the timing informations on the tracks.

## 5. – THE COSMIC RAYS VETO SYSTEM

The process $e^+e^- \rightarrow \bar{n}n$ can be simulated by interaction of cosmic muons and neutrons in the detector. Although their rate is not so high (150 Hz in coincidence with the machine radio frequency signal), they still can constitute a relevant background to $\bar{n}$ n events, whose expected rate is ~$10^{-4}$ Hz at the typical ADONE luminosity of ~ $10^{29}$ $cm^{-2}$ $s^{-1}$. To reduce this source of background a thick concrete box covered by an active veto system has been built around the detector (Fig. 1a). The concrete shield, reinforced with barium, attenuates the neutron flux and helps in containing all particles from $e^+e^-$ interactions that otherwise would lead to a self–veto. The active detector is made of Resistive Plate Counters (RPC) [19]. They consist of two parallel plane electrodes of high resistivity ($10^{11}$ Ω/cm) 2 mm apart. A 4–5 KV/mm electric field is manteined between them. The gas mixture is 69% argon, 30% butane and 1% freon. The signals are induced on 3 cm wide aluminum strips. The typical pulse amplitude is 1 V/50 Ω, the duration is 10 ns and the time spread is 1 ns. The basic RPC module has dimensions of 2x1 $m^2$ and two such modules are superimposed to form a rigid structure. A veto counter is made with three of the above described double layer structures giving a total covered area of 6x1 $m^2$. Read–out strips, 6 m long, are glued on each side of the counter and carry signals from each RPC plane. The intrinsic efficiency per plane is 97%, however the overall efficiency is increased using the logic sum of the two planes. A suitable superposition of adjacent counters has been adopted to reduce the dead space.

## 6. – THE TRIGGER

As already pointed out, the problem of the signal to background ratio is extremely important. It is thus necessary to have an efficient trigger system capable to improve this ratio to acceptable values. The FENICE first level trigger is based exclusively on signals coming from the scintillator counters.

Three types of trigger are implemented:

- $\bar{n}$ trigger ;
- trigger on two charged tracks;
- trigger on multi–hadrons.

The $\bar{n}$ trigger is based on the identification of an annihilation star. The signature of such an event is a large number of scintillators hit in a limited region of the detector. For this reason the adjacent scintillators have been grouped together to form "trigger regions", see Fig. 6. Each

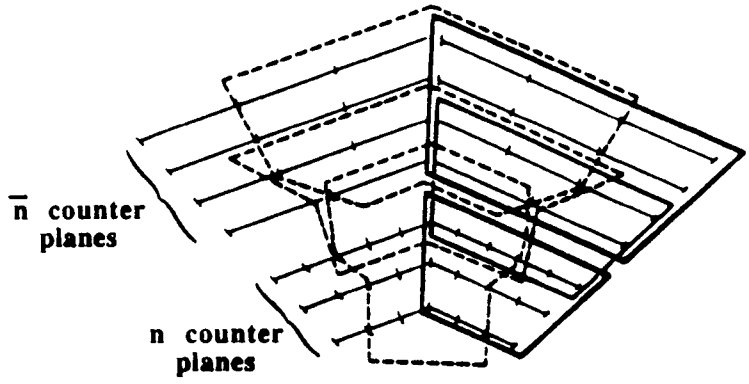


**FIG. 6** – Antineutron trigger regions: scintillator planes of two octants are schematized with straight lines.

scintillator belongs to more than one group, in order to avoid dead zones. This has been accomplished sending the signal coming from each scintillator to Mixing Box modules behaving as fan–out circuits. A Mixing Box is a passive module that reorders the signals of the scintillators belonging to the same group. Then all the signals of a defined zone are sent to a Majority Logic Unit that gives an output only when the number of input signals is greater than a fixed threshold. In order to increase the trigger selectivity also a number of photomulpiers fired ($N_{PH}$) in the whole apparatus greater than 20 is requested. To complete the requests for this trigger it is necessary to have a radio frequency signal in coincidence and no signal from the cosmic veto counters. To optimize the $\bar{n}$ trigger efficiency Monte Carlo simulations have been performed and the results are reported in Table I.

**TABLE I** – Antineutron trigger efficiency ($\varepsilon_{trig}$) is reported toghether with the fraction ($f_{ann}$) of antineutron that annihilate inside the detector for different center of mass energies.

| $E_{c.m.}$ (GeV) | $f_{ann.}$(%) | $\varepsilon_{trig.}$ (%) |
|---|---|---|
| 1.9 | 93.6 | 90.8 |
| 2.0 | 87.1 | 83.8 |
| 2.1 | 85.1 | 80.6 |
| 2.2 | 83.4 | 78.6 |
| 2.3 | 82.7 | 78.1 |
| 2.4 | 81.5 | 78.2 |
| 3.1 | 61.1 | 58.0 |

The trigger on two charged particles, mainly necessary to identify $e^+e^- \rightarrow \mu^+\mu^-$ and $e^+e^- \rightarrow e^+e^-$ reactions, asks for two collinear tracks starting from the interaction region in coincidence with a radio frequency signal and with a signal from the internal TOF system. A track is identified by a group of aligned scintillators belonging to different planes.

The multi–hadronic trigger requires many groups of scintillators fired. The considered groups are either those used to identify an antineutron or those which define a track for the trigger on two charged particles, due to the high multiplicity of a multi–hadronic event. A block scheme of the trigger configuration is reported in Fig. 7.

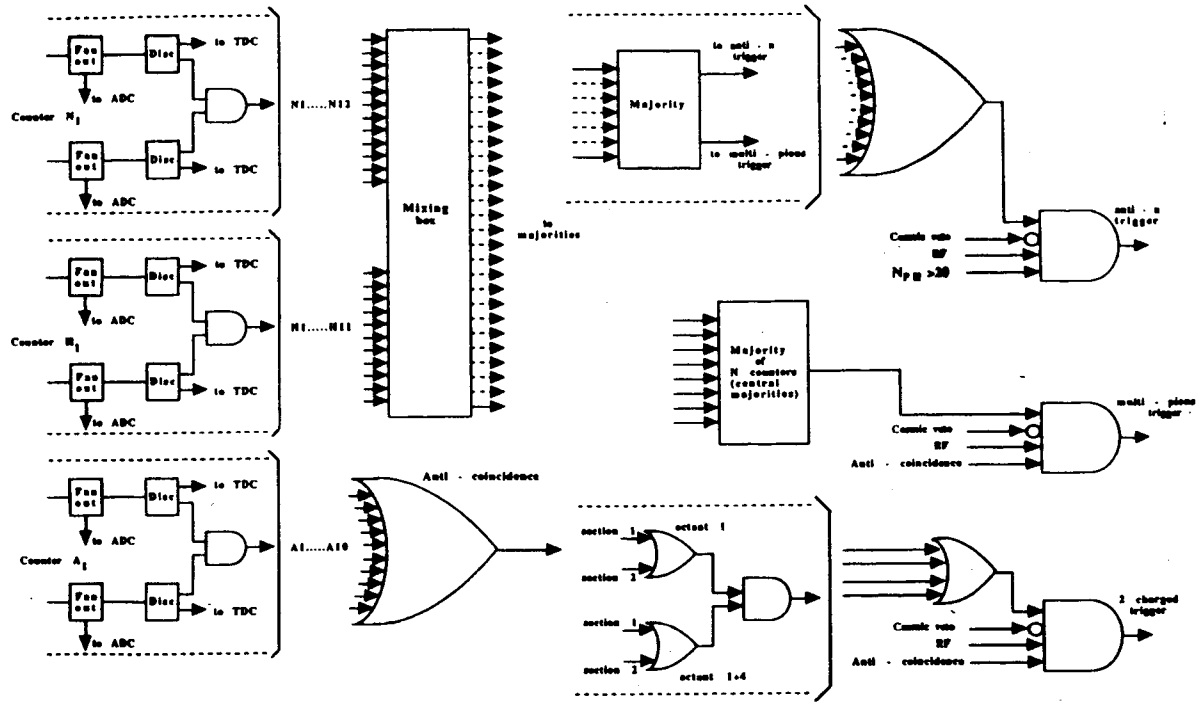


**FIG. 7** – Block scheme of the FENICE trigger configuration.

The typical efficiencies for the triggers described above at the J/Ψ energy, evaluated by Monte Carlo, are:

- 49% for the $e^+e^-$ trigger;
- 68.8% for the $\mu^+\mu^-$ trigger;
- 94.5% for the multi–hadronic trigger.

The typical counting rates at a luminosity ~ $10^{29}$ $cm^{-2}$ $s^{-1}$ and at 2 GeV center of mass energy are reported in Table II.

**TABLE II** – Typical trigger counting rates.

| | |
|---|---|
| $\bar{n}$ trigger | 10÷30 Hz (depending on the beam current) |
| trigger on two charged tracks | 0.5 Hz |
| trigger on multi–hadrons | 0.5 Hz |

In Fig. 8a,b,c and d, some typical FENICE events are displayed.

a)

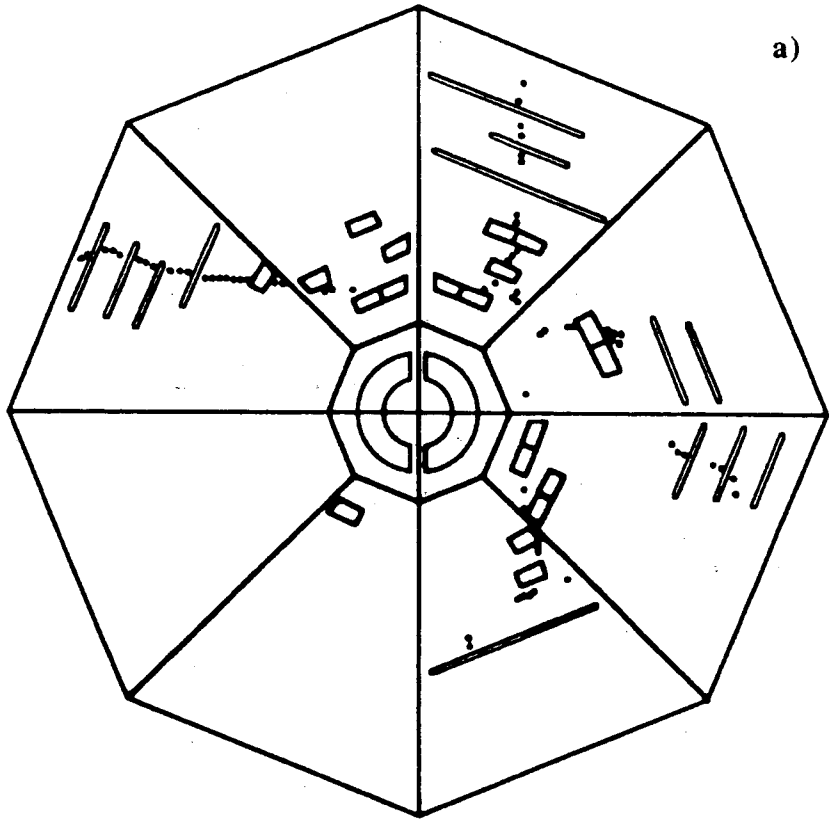

b)

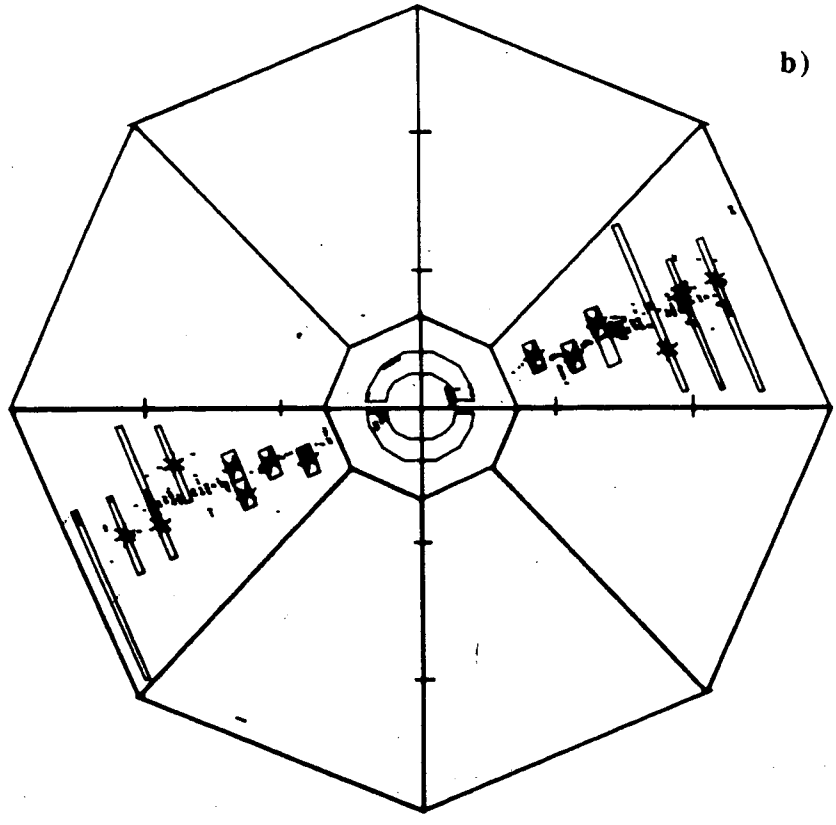

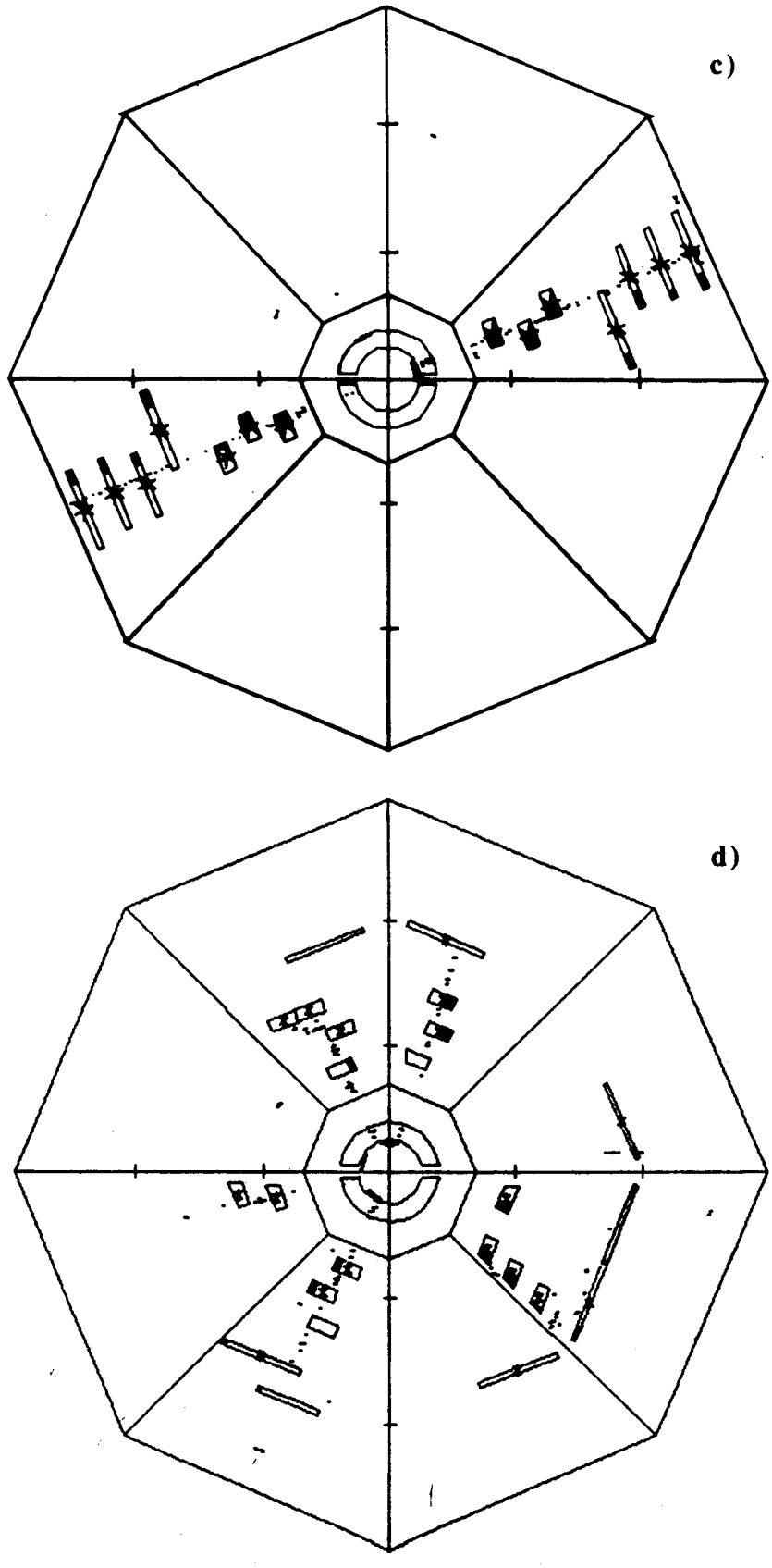


**FIG. 8a,b,c** – Display in the transverse plane of typical $\bar{n}$ n (a), $e^+e^-$ (b), $\mu^+\mu^-$ (c) and multihadronic (**d**) events. Black dots indicate the LST hits while rectangules indicate the fired scintillators.

A second level trigger, that analyzes the signals from the streamer tubes of the central detector, has been implemented for charged particles coming from the interaction region. It is based on associative memories (MEMA) and consists of a module that logically can be divided into two parts: a bank of associative memories and a controller circuit. The former is the heart of the system, where the incoming signals are compared with a set of stored patterns of physical significance. If the configuration of the event fits one of those recorded a trigger signal is produced within 18.4 μs after STROCs readout. The controller is the interface between the circuit and the rest of the world. It receives commands and loads the right configuration inside the memories.

## 7. – LUMINOSITY MEASUREMENT

The luminosity is measured by detecting the Bhabha scattering events into the experimental apparatus. Events with two collinear showers are selected using mainly the LST's pattern information. In Fig. 9 the distribution of the ratio between the number of fired strips and the crossed LST planes in both neutron and antineutron detectors is reported showing a clear discrimination between $e^+e^- \rightarrow \mu^+\mu^-$ and $e^+e^- \rightarrow e^+e^-$ events. Furthermore the $e^+e^- \rightarrow \gamma\gamma$ background events are rejected using the total number of longitudinal and transverse fired strips in CTD (Fig. 10). Fig. 11 shows the $\cos\theta$ distribution of the selected events at a center of mass energy of 3.1 Gev compared with the theoretical differential cross section $d\sigma/d\cos\theta$ .

The uncertanty on the luminosity measurement is about 5% , mainly systematic due to the evaluation of the selection efficiency.

Within this limit it also agrees with the ADONE luminosity measurement obtained by means of the reaction $e^+e^- \rightarrow e^+e^-\gamma$ [20].

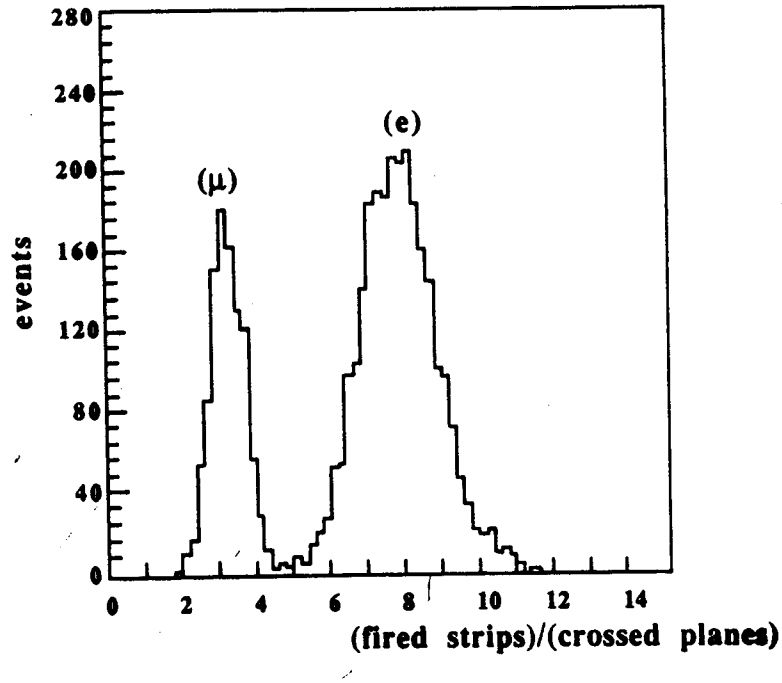


**FIG. 9** – Distribution of the ratio between the number of fired strips and the crossed LST planes for two prongs events.

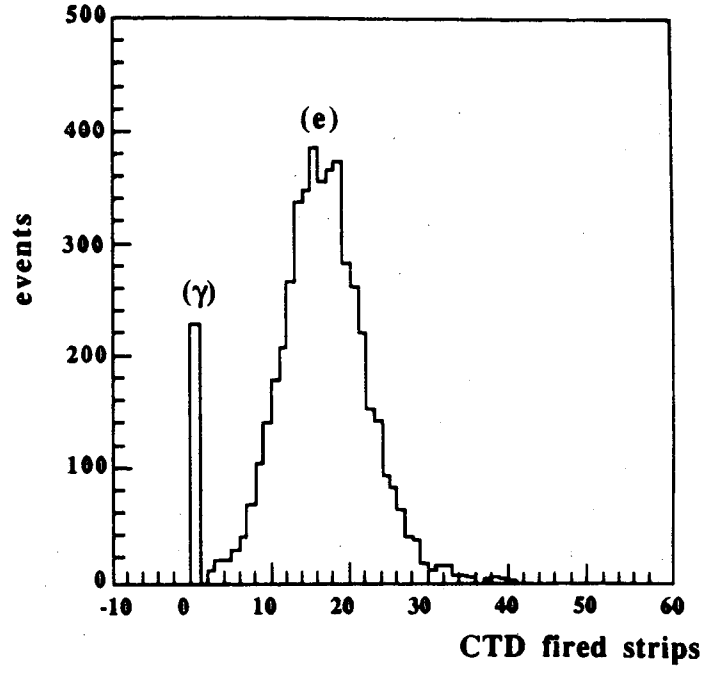


**FIG. 10** – Distribution of the total number of longitudinal and transverse fired strips in the central tracking detector for two prongs events.

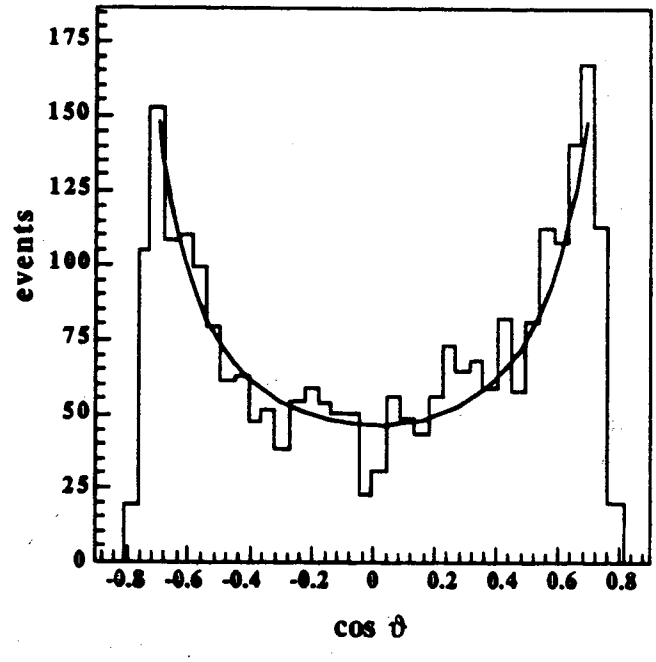


**FIG. 11** – Cosθ distubution for the $e^+e^- \rightarrow e^+e^-$ selected events. The superimposed curve is the expected QED $e^+e^-$ differential cross-section.

## 8. – THE DATA ACQUISITION SYSTEM AND THE OFF-LINE FILTERS

The Data Acquisition (DAQ) architecture of the FENICE experiment has been designed with the help of the SA/SD methodologies in order to satisfy different requirements:

- the large number of electronics channel;
- the complex LST readout cabling;
- the necessity of on–line event filtering, validation and compression;
- the high background due to the antineutron trigger.

The chosen solution [21] is schematized by Fig. 12.

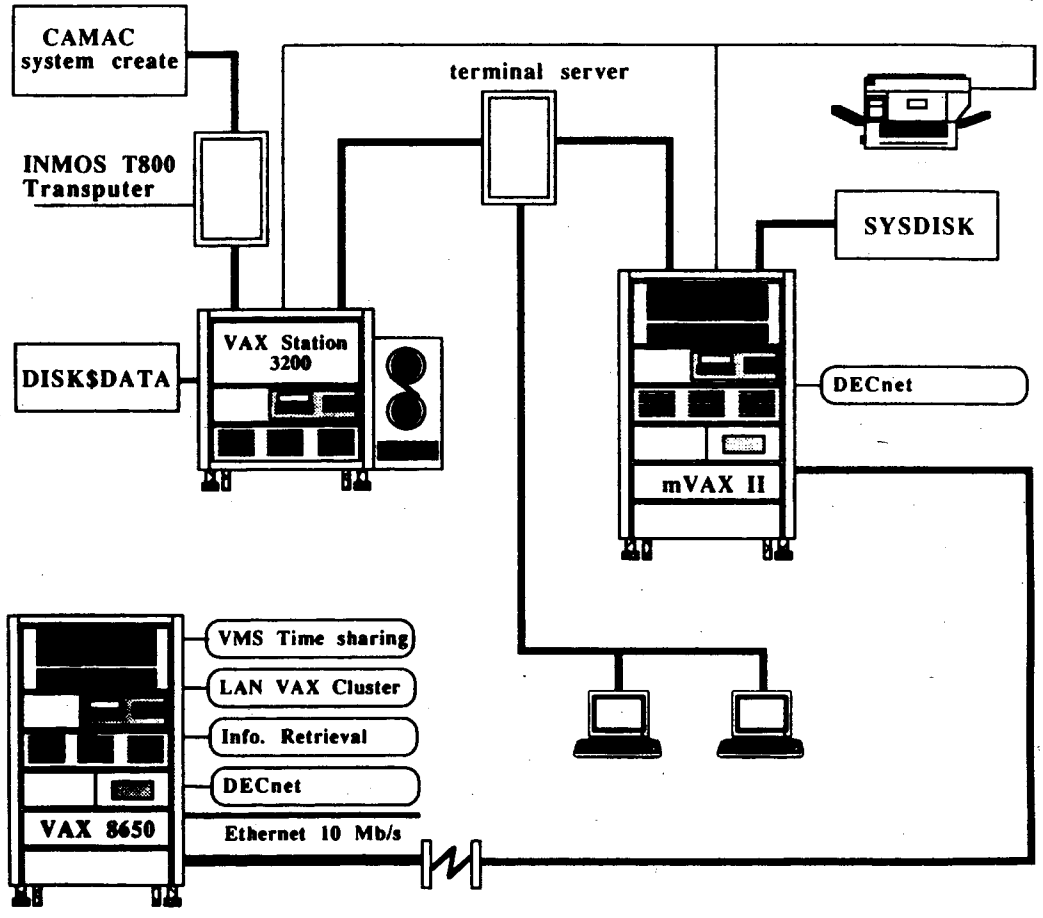


**FIG. 12** – Block diagram of the FENICE Data Acquisition scheme.

All the analog signals, coming from the Front End Electronics (FEE), are digitized, when a trigger signal occurs, in less than 200 μs. Data stored in Camac modules are then readout through a Camac branch driver by an INMOS T800 transputer and put into a circular buffer. A second transputer, hosted in the same VME module, packs the events into a 64Kb buffer and sends them to a MicroVax 3200. The readout dead time is of the order of 2 ms and it is almost entirely due to the time taken to access the Camac modules. On the MicroVax data are checked for consistency, compacted and stored onto exabyte tapes. Meanwhile two additional Vaxstations, which take part in the on–line cluster, perform monitoring and control tasks.

Camac modules are also directly interfaced to the MicroVax where all the test and setup software has been developed. They can be simultaneously accessed both by transputer and by the MicroVax via a special switching box.

The standard DAQ services (buffer management, run control, error handling, data recording) are provided by many processes running in the environment of the Fermilab VaxOnline DAQ system. Furthermore they perform specifically the following tasks:

- on–line selection of $e^+e^-$ and multi–hadron candidates;
- filling of histograms;
- settingup of programmable modules;
- event display;
- HV monitoring and control;
- run information book–keeping;
- detector calibrations;
- management of the information regarding the apparatus.

The coherence of the system is guaranteed by the convention that all the processes in the on–line system are driven by the information stored in a unique central database. This database contains data about the experiment geometry, electronics cabling, readout constant, etc. It is based on the ADAMO package which, though originally developed for event data handling, has proven to be useful also for organizing the information of the experiments [22].

The data flux rates of the FENICE DAQ system are $\Phi$raw = 40÷50 kbyte/s $\Phi$compacted = 5÷10 kbyte/s.

To reduce the amount of data to be analyzed an off–line filter is performed. The off–line data analysis procedure is based on both LST pattern and TOF information. A general filter allows the rejection of cosmic rays escaping the veto system and of machine background events. Then for each data sample $e^+e^-$, $\mu^+\mu^-$ and multi–hadrons events are selected for monitoring purposes. Finally , parallel selection for $\bar{n}n$ and $\bar{p}p$ channels are performed on the remaining events. The overall rejection factor of the off–line filters is in the range $10^3$÷$10^4$ depending on the run conditions.

After this, the selected $\bar{p}p$ , $\bar{n}n$ samples are visually inspected by means of an Event Display reconstruction program. The overall efficiency of the selection procedure is in the range 20% ÷ 40% for $\bar{n}n$ and 40% ÷ 60% for $\bar{p}p$ events depending on the center of mass energy.

## 9. – CONCLUSIONS

A non magnetic detector based on simple but reliable techniques, such as LST and scintillators, has been built at the ADONE storage ring in Frascati. It has been working from 1990 up to 1993 showing good performances fully consistent with those forseen in the design. The apparatus exibited also a high degree of stability, both in short and long term. Interventions for repairing or substituting defective parts were reduced to a minimum after the first, rather fast, debugging stage. A total of ~$10^8$ events in the c.m. energy interval from the $e^+e^- \rightarrow \bar{n}n$ threshold up to the J/$\Psi$ has been collected and are currently being analyzed. First physics results have been already published [16].

The preliminary results look very promising in getting a first insight into a field were the data are scarce or totally absent.

**Acknowledgments**

We wish to thank A. Di Biagio and A. Lucci for the skillful work on the veto counter.

## REFERENCES

[1] M.Castellano et al., Nuovo Cim. A14 (1973) 1.
[2] B.Delcourt et al., Phys. Lett. B86 (1979) 395.
[3] D.Bisello et al., Nucl. Phys. B224 (1983) 379.
[4] G.Bassompierre et al., Phys. Lett. B68 (1979) 477.
[5] A.Castro, Nucleon Structure Workshop, Frascati (1988) not published.
[6] A.Antonelli et al., Proc. LEAP90, Stockolm(1990).
[7] R.Baldini Ferroli and M.E.Biagini, Internal note LNF– 89/090 (P) (1989).
[8] N.Cabibbo, R.Gatto, Phys. Rev. 124 (1961) 1577.
R.Felst, Internal note DESY 73/56 (1973).
J.G.Korner and M.Kuroda, Phys. Rev. D 16 (1977) 2165.
P.Ceselli, M.Nigro, C.Voci, Proc. Workshop on Physics at LEAR, Erice (1982).
E.Etim and A.Malecki, Internal note LNF–89–023 (1989).
S. Dubnicka, Nuovo Cimento A100 (1988) 1, A103 (1990) 469, A104 (1991) 1075.
S.I.Bilenkaya, S.Dubnicka, A.Z.Dubnickova and P.Strizenec, Nuovo Cimento A105 (1992) 1.
[9] V.L.Chernyak and I.R.Zhitnitski, Nucl. Phys. B 206 (1984) 52.
S.J.Brodsky, Proc. Nucleon Structure Workshop, Frascati (1988) not published.
T.Hyer, Preprint SLAC–pub–5889 (1992).
[10] F.Amman et al., Proceeding Int. Acell. Conf., Geneva (1971).
[11] T.Bressani et al., IEEE trans. on N.S. 32 (1985).
[12] T.Bressani et al., Nucl. Instr. Meth. A292 (1990) 563.
[13] G.Battistoni et al., Nucl. Instr. Meth 164 (1979) 57.
[14] M.Spinetti, Proc. second Winter School on Hadronic Physics, Folgaria (1987) 409.
[15] A. Cavestro et al, Nucl. Instr. Meth. A312 (1992) 571.
[16] A.Antonelli et al., Phys. Lett. B301 (1993) 317.
A.Antonelli et al., Internal Note LNF93 / 031P (1993).
[17] P. Macciotta et al., IEEE trans. on N.S. 33 (1986).
[18] M.Morandin, PHD Thesis Universita' degli studi di Padova (1985/1986).
[19] R.Santonico and R.Cardarelli; Nucl. Instr. Meth 187 (1981) 377.
[20] H.C Dehne et al., Nucl. Instr. Meth 116 (1974) 345.
M.Preger,Internal note ADONE SC–119 (1985).
[21] A.Antonelli et al, Proc.Computing for High Luminosity and High Intensity Facilities, Ed. J.Lillberg, M.Oothoudt, American Institute of Physics (1990) 251.
[22] A.Antonelli et al., Proc. New Computing techniques in Physics Research, Ed. D.Perret–Gallix, W.Wojcik, Editions du Centre National de la Recherche Scientifique Paris (1990).
[23] CERN Note DD / EE / 84–1 (1991)